Push the Limit of Millimeter-wave Radar Localization

GUIDONG ZHANG, GUOXUAN CHI, YI ZHANG, XUAN DING, and ZHENG YANG,
Tsinghua University, China

Existing device-free localization systems have achieved centimeter-level accuracy and show their potential in a wide range of applications. However, today's radio-based solutions fail to locate the target in millimeter-level due to their limited bandwidth and sampling rate, which constrains their applications in high-accuracy demand scenarios. We find an opportunity to break the bottleneck of existing radio-based localization systems by reconstructing the accurate signal spectral peak from the discrete samples, without changing either the bandwidth or the sampling rate of the radio hardware. This study proposes *milliLoc*, a millimeter-level radio-based localization system. We first derive a *spectral peak reconstruction algorithm* to reduce the ranging error from the previous centimeter-level to millimeter-level. Then, we improve the AoA measurement accuracy by leveraging the signal amplitude information. To ensure the practicality of *milliLoc*, we further extend our system to handle multi-target situations. We fully implement *milliLoc* on a commercial mmWave radar. Experiments show that *milliLoc* achieves a median ranging accuracy of 5.5 mm and decreases the AoA measurement error by 31.2% compared with the baseline. Our system fulfills the accuracy requirements of most application scenarios and can be easily integrated with other existing solutions, shedding light on high-accuracy location-based applications.

CCS Concepts: • **Human-centered computing → Ubiquitous and mobile computing systems and tools;**

Additional Key Words and Phrases: Millimeter-wave radar, millimeter-level localization, Angle-of-Arrival measurement

ACM Reference format:
Guidong Zhang, Guoxuan Chi, Yi Zhang, Xuan Ding, and Zheng Yang. 2023. Push the Limit of Millimeter-wave Radar Localization. *ACM Trans. Sensor Netw.* 19, 3, Article 59 (April 2023), 21 pages.
https://doi.org/10.1145/3570505

1 INTRODUCTION

Acquiring accurate location of a target is a fundamental component required by a wide range of real-world applications, such as security monitoring, virtual reality, smart homes, and asset management. For this wide range of applications, localization accuracy is a key factor that decides how prevalent the applications can be deployed and utilized. For example, being capable of tracking fingers means that we can control the channel and volume of television with our bare hands. To

This work is supported in part by the National Key Research Plan under grant No. 2021YFB2900100, the NSFC under grant No. 61832010, No. 61972131, and No. 62232004.
Authors' address: G. Zhang, G. Chi, Y. Zhang, X. Ding, and Z. Yang (corresponding author), Tsinghua University, Beijing, China; emails: zhanggd18@gmail.com, chiguoxuan@gmail.com, zhangyithss@gmail.com, dingx04@gmail.com, hmilyyz@gmail.com.

1550-4859/2023/04-ART59 $15.00
https://doi.org/10.1145/3570505

accurately use finger movements to control smart homes, we need millimeter-level localization accuracy.

In addition, some industrial applications also require high-resolution localization, including mechanical arms, conveyor belts, subway train control systems, and **tunnel boring machine (TBM)** systems. As an example, the thrust cylinders on TBM require millimeter-level accuracy to ensure precise tunnel excavation. Traditional mechanical sensors are cumbersome to deploy and prone to mechanical failures such as chain jamming, which can cause data jitter. The subway train control system also requires millimeter-level accuracy to exactly align the position of the screen door on the platform so passengers can get on and off the train normally.

Over the past decades, pioneer efforts have been devoted to accurate target localization and tracking. However, some of them require the target to carry dedicated devices, such as RFID tags [34, 45], mobile phones [17, 21, 31, 39, 49], and wearable devices [11, 12], which poses inconvenience and even infeasibility under specific scenarios. As such, device-free localization, which is also called passive localization, attracts increasing research interest, as it does not need any device attached to the target. Mainstream researches focus on utilizing cameras, Wi-Fi, or sound signal for localization. Among all existing device-free localization techniques, camera-based solutions [9, 48] have limitations of adequate illumination and raise serious privacy concerns. Wi-Fi-based solutions [20, 25, 41, 42] are promising, thanks to the unique advantages of Wi-Fi in its ubiquitous deployment. However, suffering from their limited meter-level accuracy, these solutions are insufficient to support high-accuracy location-based services. Sound-based systems [36, 46] usually have a small coverage area and deteriorate under noise surroundings due to lower input SNR.

Compared with the aforementioned solutions, **millimeter-wave (mmWave)** devices offer a higher resolution. By taking advantage of the unique reflected target features and advanced denoising methods, existing mmWave-based localization systems, such as mmTrack [40] and WiTrack2.0 [5] have made a promising step towards decimeter-level location accuracy. However, their localization accuracy is still affected by limited bandwidth and can not be further improved. mmVib [13] and Osprey [24] can achieve millimeter-level and even sub-millimeter-level sensing, but they pay more attention to the displacements of targets during movements, rather than the absolute range.

More importantly, the accuracy of the absolute range is still limited by signal bandwidth and sampling rate.[1] We extract the signal frequencies to acquire the absolute range by **Discrete Fourier Transform (DFT)**, and the sampling error has a significant negative impact on distance measurement. As shown in Figure 1, the real frequency of the signal is f_0, but due to frequency sampling, we consider the signal frequency is $f_0^{'}$, which causes frequency error δ. Consequently, there is an "ambiguity area" in the frequency calculation, and the frequencies in the "ambiguity area" will be regarded as the same frequency $f_0^{'}$. As introduced in Section 2, the "ambiguity width," which is frequency resolution Δf, is related to the observation time. Applied to the range measurements in wireless signal, the "ambiguity" in frequency spectrum results in the "ambiguity" of range. As illustrated in Figure 1, there are range bins for the range measurements in the wireless field. Targets located anywhere in a range bin will get the same range result, which leads to the "ambiguity" of range measurements. Even though some of existing works are able to achieve higher granularity sensing, including mmVib [13] and Osprey [24], they use phase information to detect the motion of targets and do not contribute much to the measurement of the absolute range of the target. In addition, the frequency error causes the "ambiguity" of **Angle-of-Arrival (AoA)** measurements.

[1]According to the signal processing principle in Section 2, the resolution of the RF signal is inversely proportional to its bandwidth. Take the commonly used mmWave radar with 4 GHz bandwidth as an example: The range resolution is generally considered to be about 4 cm.

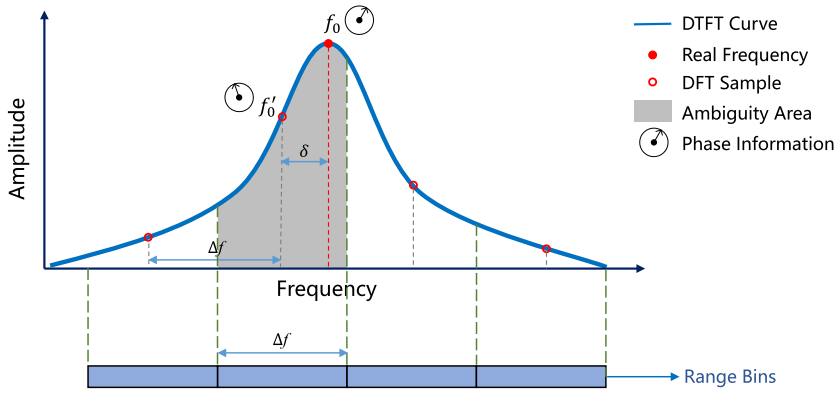

Fig. 1. The example of sampling error in the frequency spectrum. frequency error δ leads to the "ambiguity" of range measurement, and there is also a deviation between the phase of the real peak point and the sampling peak point.

According to Section 3.4, AoA is calculated by the phase of the peak point in the frequency spectrum. Owing to the frequency error, there is a deviation between the phase of the real peak point and the sampling peak point, which brings about the deviation of AoA calculation.

To break the bottleneck inherent from the signal processing theory itself, one feasible solution is to dig into the working mechanism of hardware and signal processing theory, then propose a "super-resolution" algorithm that can improve the frequency estimation accuracy. Many super-resolution works have been designed, including MUSIC [30], ESPRIT [29], and their extended techniques Ubicarse [18], D-MUSIC [26], and GPR [23]. They mostly focus on "super spatial resolution," which makes multi-path signals *distinguishable*. However, they pay more attention to the high-level algorithms and ignore low-level problems of frequency calculation. By contrast, our work pays more attention to "super frequency resolution," which makes the localization results more *accurate*. To achieve this promising solution, we address three significant challenges that require non-trivial efforts.

- **Limited range resolution.** As illustrated in Figure 1, there is "ambiguity" in the range estimation. Based on the time-frequency analysis theory, the spatial resolution of the RF signal is inversely proportional to its bandwidth. Due to the radio hardware implementation, improving the range resolution by simply increasing the signal bandwidth is unrealistic. The current range resolution can not meet the needs of millimeter-level localization.
- **Limited angular resolution.** To locate the target in a 2D polar coordinate system accurately, both the radial distance and the angle need to be precise enough. The traditional AoA calculation algorithm is based on the phase difference between multiple antennas. According to the mentioned above, frequency error during sampling inevitably suffers from the phase noise. The inaccurate AoA resolution limits the localization capability of millimeter waves in the 2-D plane.
- **Multi-target localization.** Multiple targets may appear in the monitoring area simultaneously, and their reflected signals would be superposed together. Therefore, it is challenging to identify each target's reflected signal.

To tackle the above challenges, we propose *milliLoc*, a millimeter-level multi-target localization system based on a **commercial-off-the-shelf (COTS)** mmWave device. In *milliLoc*, to improve the range accuracy, we analyze the process of the Fourier transform and then derive the *spectral peak reconstruction algorithm*, which successfully reduces the ranging error from centimeter level

to millimeter level by solving an optimization problem. On this basis, we innovatively leverage the signal amplitude information from the equations mentioned above to improve the AoA accuracy of *milliLoc*. To realize multi-target localization, we further extend *milliLoc* to separate the superposed spectrum caused by the reflections from multiple objects.

We have fully implemented *milliLoc* on commercial mmWave device IWR1443BOOST [4] with transmitted signal frequency ranges from 77 GHz to 81 GHz. Experiments show *milliLoc* could achieve a median ranging accuracy of 5.5 mm, which outperforms the conventional "peak-pt" scheme [1] by more than 50%. For the AoA measurement, *milliLoc* achieves a median accuracy of 6.6°, which precedes the traditional method with a decrease of error by 31.2%. In view of the universality of frequency calculation and sampling errors presented in most cases, we believe that our method could be applied to not only mmWave radar, but also other RF-signal-based sensing systems, including Wi-Fi signal, sound signal, and lidar. Our technique is able to boost the sensing accuracy of various RF signals, which could expand their applications.

In summary, our core contributions are as follows:

- We propose *milliLoc*, a millimeter-level multi-target localization system based on COTS mmWave device. As underlying technical support, our solutions can be integrated with other wireless sensing systems to achieve better performance.
- We push the limit of the mmWave radar's ranging accuracy to millimeter-level by deriving a novel *spectral peak reconstruction algorithm* based on our in-depth understanding of Fourier transform theory. Then, we reduce the systemic error in AoA measurement and improve the angular accuracy by innovatively leveraging the amplitude information of the received signal.
- We fully implement *milliLoc* on a COTS mmWave device and evaluate it in three different scenarios. Experiment results demonstrate that *milliLoc* achieves millimeter-level ranging accuracy and decreases the AoA measure error by 31.2%. Apart from these, our system could locate multiple targets concurrently.

The rest of the article is organized as follows: Section 2 demonstrates the FMCW signal and range resolution. Section 3 gives the system design. Experiments and evaluations are provided in Section 4. Section 5 proposes the discussion. Section 6 gives the related work followed by a conclusion in Section 7.

2 PRELIMINARY

In our work, we use a COTS mmWave device IWR1443BOOST [4] provided by TI company. As shown in Figure 2, the transmitted signals are **Frequency Modulated Continuous Wave (FMCW)** chirps, which could be formulated [1, 7] as:

$$S_{Tx}(t) = \cos\left(2\pi f_0 t + \frac{\pi B}{T_c} t^2\right), \tag{1}$$

where f_0 is start frequency, B is the chirp bandwidth, and T_c is the chirp duration. From Equation (1), the frequency of the chirp is $f_0 + \frac{B}{T_c} t$, which increases linearly along time.

The chirp signal would be reflected by targets and captured by receive antennas. The received signal could be viewed as a delayed version of transmitted chirp, which could be denoted as:

$$S_{Rx}(t) = \alpha S_{Tx}\left(t - \frac{2d}{c}\right), \tag{2}$$

where α is the signal attenuation, d is the distance between mmWave device and target, and c represents the propagation velocity of electromagnetic wave.

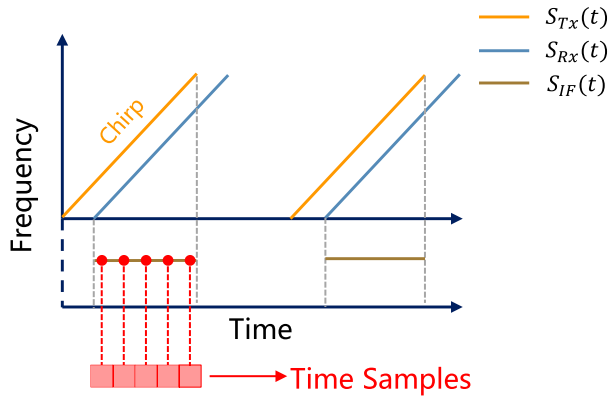

Fig. 2. The example of FMCW chirp signals.

The time delay of reflection signals could be calculated by the frequency differences between the transmitted and received signals, which can demonstrate the range information. A mixer is used to obtain the **intermediate frequency (IF)** signal. The IF signal could be illustrated as:

$$S_{IF}(t) = \hat{\alpha} \cos\left(\frac{4\pi Bd}{cT_c} t + \varphi_0\right), \tag{3}$$

where φ_0 is the initial phase. From Equation (3), we know that the frequency of IF signal $S_{IF}(t)$ is proportional to the distance between the mmWave device and the target.

To get the distance of the target, we need to extract the frequency of the IF signal. The most common way to extract frequency is to apply DFT to the IF signal. Each peak point in the spectrum represents a frequency component, which is caused by a reflection signal. The frequency resolution of DFT is $\Delta f = \frac{1}{T_c}$, where T_c is the observation time [1, 33]. Since $\Delta f = \frac{2B\Delta d}{cT_c}$, the resolution of range could be calculated by:

$$\Delta d = \frac{c}{2B}. \tag{4}$$

It shows that the range resolution is inversely proportional to the bandwidth.

IWR1443 works on the frequency range from 77 GHz to 81 GHz and the maximum bandwidth is 4 GHz. However, the available bandwidth is slightly less than 4 GHz due to bandwidth loss in practice. Consequently, the range resolution of the method is around 4 cm. It means that if a target locates anywhere in the range bin with 4 cm, then the mmWave device would give the same range results, which means the "ambiguity" in range estimation.

3 SYSTEM DESIGN

3.1 System Overview

As introduced in Section 2, we could use the peak point in the IF frequency spectrum to estimate the frequency. However, the frequency resolution is limited by signal observation window size, which restricts the range resolution in the target localization of FMCW radar.

For example, there are two discrete sine signals as shown in Figure 3: $s_1[n] = A_1 e^{j\theta_1} e^{j2\pi f_1 n}$ and $s_2[n] = A_2 e^{j\theta_2} e^{j2\pi f_2 n}$, where $A_1 e^{j\theta_1}$ and $A_2 e^{j\theta_2}$ are amplitudes; $f_1 = \frac{k_p - \delta}{N}$ and $f_2 = \frac{k_p + \delta}{N}$, which are normalized frequencies defined in $[0, 1]$; N is the sample number and δ is a real number in $[-\frac{1}{2}, \frac{1}{2}]$. Although the frequencies of s_1 and s_2 are not exactly equal, they have the same bin index with maximal amplitude in the DFT spectrum at k_p due to sampling error of DFT. In other words,

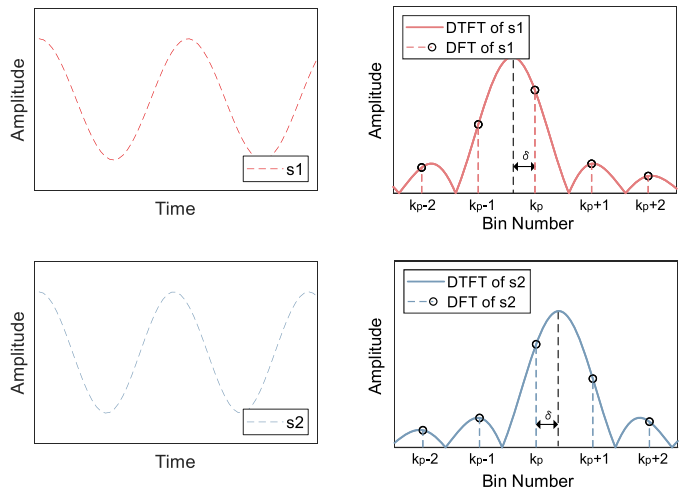

Fig. 3. Examples of DFT frequency resolution.

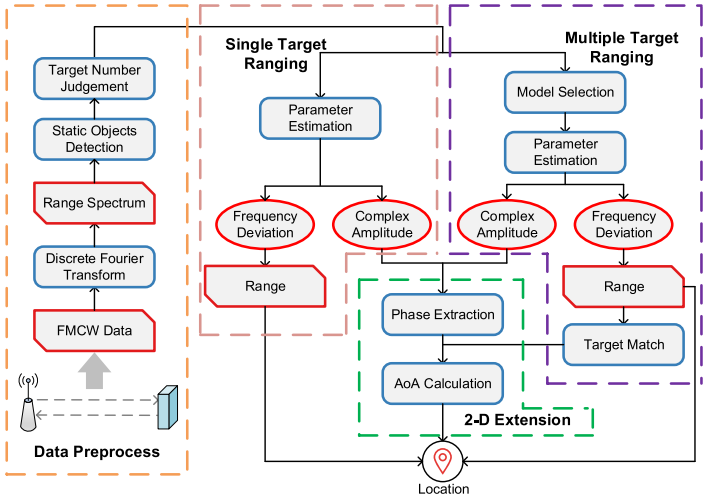

Fig. 4. System overview of *milliLoc*.

s_1 and s_2 both lie in the same "ambiguity area." We would determine that s_1 and s_2 have the same frequency and ignore their slight distinctions by the mentioned method above.

Nevertheless, the DFT amplitude distributions of s_1 and s_2 are not identical. For instance, their spectrum amplitudes of bin $k_p - 1$, k_p and $k_p + 1$ are varied, even though they have the same bin index with maximal amplitude. If we make full use of the information of DFT results rather than only choosing a peak point, then we might get more accurate frequency information. Applying to target ranging based on FMCW mmWave radar, we are capable of obtaining higher range accuracy. We will establish the quantitative analysis model, consider the noises under the actual situation, and propose our method based on the above idea.

Figure 4 illustrates *milliLoc*'s overall architecture. We preprocess the raw FMCW data as introduced in Section 2 and then obtain the range spectrum. During target ranging, reflections from other static objects may be received by mmWave device, which would interfere with target

detection and ranging. To reduce the influence of static objects, we collect data in the experimental environment in advance and analyze the distribution of static objects to reduce their impact on target ranging [37].

After static objects detection, we could calculate the number of targets based on the existing work [1, 38]. In view of the single-target and multi-target situations, we propose the single target ranging scheme and multiple targets ranging scheme, which would be elaborated in Sections 3.2 and 3.3, respectively. We give a *spectral peak reconstruction algorithm*, which models the output signal of mmWave radar and derives the accurate range by solving an optimization problem. For multiple targets, we extend *milliLoc* to separate the superposed spectrum caused by the reflections from multiple objects. By the amplitude information acquired in equations, we improve the AoA accuracy and achieve 2D localization, which is provided in Section 3.4.

3.2 Single Target Ranging

For ease of understanding, we first consider the most basic scenario with only one target. We propose a *spectral peak reconstruction algorithm* to acquire the accurate frequency. Based on the previous analysis, one target means the reflected Rx signal contains only one frequency component. Then, we will give the theoretical model with only one frequency component.

A single-frequency complex discrete signal under white Gaussian noise could be modeled as follows:

$$r[n] = A_0 e^{j\theta_0} e^{j2\pi f n} + w[n], n = 0, 1, \ldots, N-1, \tag{5}$$

where $A_0 e^{j\theta_0}$ is the unknown complex-valued amplitude, A_0 and θ_0 both are real numbers, $f = \frac{k_p+\delta}{N}$ is the normalized frequency defined in $[0, 1]$, δ is a real number in $[-\frac{1}{2}, \frac{1}{2}]$, N is the sample number, and $w[n]$ is white Gaussian noise. Our goal is to estimate δ in the DFT spectrum to get a more accurate signal frequency.

DFT of $r[n]$ could be calculated by [33]:

$$R[k] = \sum_{n=0}^{N-1} r[n] e^{-j\frac{2\pi}{N}nk}, k = 0, 1, \ldots, N-1. \tag{6}$$

Generally, the **signal-to-noise ratio (SNR)** is sufficiently large, and we could presume that k_p corresponds to the bin index with maximal amplitude in the DFT spectrum. Consequently, there are three unknown real parameters in the signal: A_0, θ_0, and δ.

From Equations (5) and (6), we could give the DFT results as follows:

$$\begin{aligned} &R[k_p - m] = A_0 e^{j\theta_0} \frac{1-e^{j2\pi(\delta+m)}}{1-e^{j\frac{2\pi}{N}(\delta+m)}} + W[k_p - m], \\ &m = k_p - N + 1, k_p - N + 2, \ldots, k_p, \end{aligned} \tag{7}$$

where $W[k_p - m]$ is the DFT of $w[n]$.

Considering that DFT results $R[k]$ are complex values, the real part and imaginary part of Equation (7) are equal, respectively. In other words, Equation (7) could be decomposed into two equations of real numbers:

$$\begin{aligned} &\text{Real}\{R[k_p - m]\} = \text{Real}\left\{A_0 e^{j\theta_0} \frac{1-e^{j2\pi(\delta+m)}}{1-e^{j\frac{2\pi}{N}(\delta+m)}} + W[k_p - m]\right\}, \\ &\text{Imag}\{R[k_p - m]\} = \text{Imag}\left\{A_0 e^{j\theta_0} \frac{1-e^{j2\pi(\delta+m)}}{1-e^{j\frac{2\pi}{N}(\delta+m)}} + W[k_p - m]\right\}, \\ &m = k_p - N + 1, k_p - N + 2, \ldots, k_p. \end{aligned} \tag{8}$$

Equation (8) shows that each DFT sample could provide two real equations.

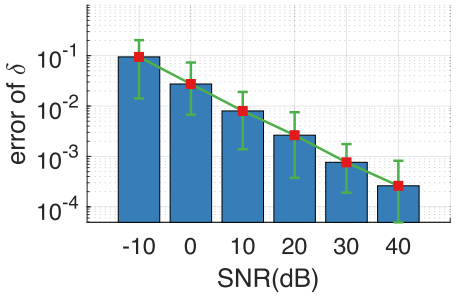

Fig. 5. Single-frequency signal estimation error of frequency derivation δ with respect to SNR.

In our problem, at least two DFT samples are needed to solve a system of nonlinear equations for three unknown real parameters. Theoretically, the solution would be more precise if more DFT samples are used. The process of solving the system of nonlinear equations is equivalent to solving the following optimization problem:

$$\min_{(A_0,\theta_0,\delta)} \left\langle R[k] - A_0 e^{j\theta_0} \frac{1 - e^{j2\pi(\delta+k_p-k)}}{1 - e^{j\frac{2\pi}{N}(\delta+k_p-k)}} \right\rangle, k = K_1, K_2, \ldots, K_N, \tag{9}$$

where $K_1, K_2, \ldots, K_N$ are DFT samples involved in the solution, and $\langle \bullet \rangle$ represents the real part or imaginary part. However, some DFT samples with lower magnitude would have larger errors due to interference of noise. To reduce the influence of noise, we apply amplitude modulation to the optimization problem. In detail, we use the amplitude of samples to adjust the coefficients of the optimization problem. Thus, samples with lower amplitude make less contribution to the solution of the optimization problem, which would relieve the disturbance of noise. Consequently, we solve the optimization problem as follows:

$$\min_{(A_0,\theta_0,\delta)} |R[k]| \left\langle R[k] - A_0 e^{j\theta_0} \frac{1 - e^{j2\pi(\delta+k_p-k)}}{1 - e^{j\frac{2\pi}{N}(\delta+k_p-k)}} \right\rangle, k = K_1, K_2, \ldots, K_N. \tag{10}$$

Therefore, we select the DFT samples with higher amplitude and solve the optimization problem by Levenberg–Marquardt algorithm, a common method for the solution of certain nonlinear problems in least squares [19, 22]. Consequently, we obtain the complex-valued amplitude $A_0 e^{j\theta_0}$ and more accurate frequency $\frac{k_p+\delta}{N}$. Then, we could calculate the target range refer to:

$$d = \frac{k_p + \delta}{N} \frac{cF_s T_c}{2B}, \tag{11}$$

where F_s is the sample rate of mmWave device.

The method is evaluated through simulation. We preset a single-frequency signal and add white Gaussian noise with different power according to SNR. Then, we estimate frequency derivation δ by the above-mentioned method. Figure 5 shows the estimation error with respect to various SNR. The estimation error of δ declines gradually with the increase of SNR. Even with an SNR of 10 dB, we achieve a median error of 0.01 in δ. As presented in Section 2, the normalized frequency estimation error of 1 represents the localization error of 4 cm. Consequently, our method is able to achieve a median localization error of 0.4 mm with the SNR of 10 dB under ideal conditions.

We analyze the process of Fourier transform and give the *spectral peak reconstruction algorithm*, which builds and solves an optimization problem to obtain the accurate frequency. Simulation results show that our approach is able to acquire more fine-grained frequency estimation results.

During the movement of the target, secondary reflections from the target might disturb normal localization. In addition, sometimes the targets produce strong specular reflections (similar to a

mirror) to the incident mmWave signal, and reflected signals are not always captured by the receive antennas, which would deteriorate localization accuracy [6, 8]. We can use the continuity of distance over adjacent frames to reduce the impact of various external disturbances [38]. We analyze the localization of the target during the overall monitoring period, and correct the localization results with larger deviations according to adjacent frames, which would reduce the influence of accidental errors and external noise.

Considering that common radar equipment usually has a high SNR, even with more complex noise rather than white Gaussian noise, we are confident to achieve millimeter-level localization error.

3.3 Multiple Target Ranging

In practical applications, however, multiple targets may appear at the same time, which may cause performance degradation and further constrain the application scenarios of cargo spotting devices where multiple targets need to be located. To tackle this complex situation, we innovatively derive a multi-frequency signal algorithm. For ease of understanding, here, we consider a double-frequency signal as an example.

A double-frequency complex discrete signal under white Gaussian noise could be written as follows:

$$t[n] = A_1 e^{j\theta_1} e^{j2\pi f_1 n} + A_2 e^{j\theta_2} e^{j2\pi f_2 n} + w[n], n = 0, 1, \ldots, N-1, \tag{12}$$

where $A_1 e^{j\theta_1}, A_2 e^{j\theta_2}$ are unknown complex-valued amplitudes, $f_1 = \frac{k_{p1}+\delta_1}{N}, f_2 = \frac{k_{p2}+\delta_2}{N}$ are normalized frequencies, N is the sample number, and $w[n]$ is white Gaussian noise.

As presented in Section 3.2, we could calculate the DFT spectrum $T[k], k = 0, 1, \ldots, N-1$ by Equation (6) and read the value of k_{p1}, k_{p2}. Now, we have six unknown real parameters in the double-frequency signal, including $A_1, A_2, \theta_1, \theta_2, \delta_1, \delta_2$.

In the single-frequency signal, we use at least two samples with higher magnitude in the DFT spectrum to solve unknown parameters. In the double-frequency signal, we consider two different situations:

- If $|k_{p1} - k_{p2}| > 3$, which there is a large difference between the frequencies f_1 and f_2, then we solve the parameters of each frequency component separately. Here, the mutual influence between two frequency components is slight.
- If $|k_{p1} - k_{p2}| \leq 3$, then the peaks of two frequency components in the DFT spectrum would be jumbled together. It will bring larger error to calculate the parameters of each frequency component separately, as introduced in Section 3.2. Consequently, We solve the whole unknown parameters in one optimization problem. Considering that there are six unknown real parameters, we need at least six real equations, i.e., three DFT sampling point information to form a system of nonlinear equations to establish the optimization problem. Because there are two components, which peak points in the frequency spectrum locate at k_{p1} and k_{p2}. We need to distinguish the magnitude of k_{p1} and k_{p2} to make it clear that "we use the DFT spectrum results from '$T[k_{p1}-1]$ to $T[k_{p2}+1]$' or '$T[k_{p2}-1]$ to $T[k_{p1}+1]$". Consequently, we suppose that $k_{p1} \leq k_{p2}$ to determine an explicit DFT spectrum result range.

If more frequency components exist in the signal, then we solve the parameters by the above mentioned method. If the components do not have closer frequencies, then we solve each frequency component, respectively. If the components have closer frequencies, then we solve them by a unified optimization problem. To settle a system of equations with u frequency components, i.e., $3u$ unknown parameters synchronously, we need $3u$ equations and $\lceil \frac{3}{2}u \rceil$ DFT samples.

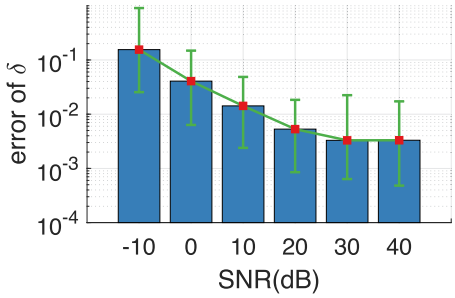

Fig. 6. Double-frequency signal estimation error of frequency derivation δ with respect to SNR when there is a large difference between the frequencies of two components.

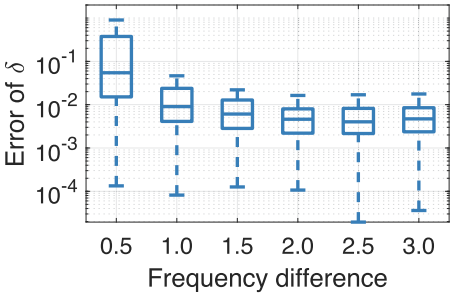

Fig. 7. Double-frequency signal estimation error of frequency derivation δ with respect to various frequency difference for SNR $= 20dB$ when the frequencies of two components are similar.

We preset a signal with two frequency components as well as white Gaussian noise. When the two bin indexes with maximal amplitude are larger than 3, which means the distance between two targets surpasses 12 cm, we calculate each frequency component separately, and Figure 6 shows the simulation performance. When SNR surpasses 20 dB, the error of δ exceeds which in a single-frequency situation. It is because the white Gaussian noise is lower and a frequency component would interfere with another frequency component. However, white Gaussian noise dominates the whole interference when SNR $<$ 20 dB, which accounts for almost the same estimation performance between single or double frequency components. Overall, the error of frequency estimation results remains at low levels, which shows the effectiveness of our system.

When the two bin indexes with maximal amplitude are smaller than 3, which means the distance of two targets does not exceed 12 cm, we need to calculate two frequency components in one optimization problem. We evaluate the error of δ with respect to the normalized frequency difference between two frequency components and the SNR is fixed to a specific value, which is 20 dB. As shown in Figure 7, our algorithm resolves two frequency components successfully when the normalized frequency difference is larger than 1. When two frequencies get too close to each other, our method could not distinguish different components and generate a large estimation bias. This is because there are few samples with higher amplitude, and samples with lower amplitude are vulnerable to system noises, which leads to less accurate estimation results.

We select different optimization problems to solve multiple-target localization according to their location relationship. Simulation results show that our method is capable of separating different frequency components.

3.4 2D Extension

Although *milliLoc* has achieved mm-level ranging accuracy, in most cases, we need to acquire the target's 2D localization. To realize an accurate 2D localization, the AoA estimation needs to be further improved.

milliLoc uses linear Rx antenna array on mmWave radar to calculate AoA. Figure 8 shows a simple 3-antenna linear array with d_0 distance separation. Usually, the distance between target and device $d \gg d_0$, hence the reflected signals reach the antenna array almost in parallel. From geometrical relationship, the distance difference between adjacent antennas $\Delta d = d_0 \sin\theta$, where θ is AoA of the receiving signal. The phase difference between adjacent antennas could be represented as [42]:

$$\Phi = \frac{2\pi d_0 \sin\theta}{\lambda}, \tag{13}$$

where λ is the wavelength. We could calculate target AoA by Equation (13) in theory.

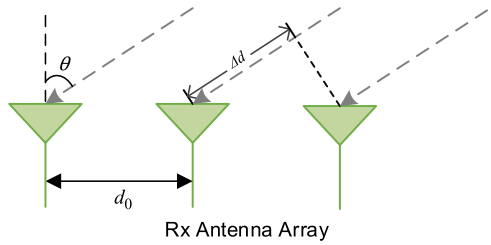

Fig. 8. Uniform linear array to calculate AoA.

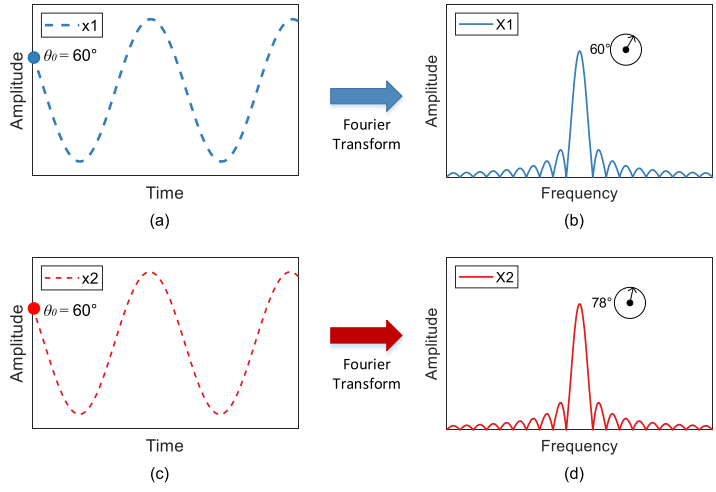

Fig. 9. The examples that extract the initial phase by DFT. (a) The real part of $x_1[n]$, where frequency deviation $\delta = 0$. (b) The DFT result of $x_1[n]$. the phase of peak point is equal to the initial phase of $x_1[n]$. (c) The real part of $x_2[n]$, where frequency deviation $\delta \neq 0$. (d) The DFT result of $x_2[n]$. the phase of peak point is not equal to the initial phase of $x_2[n]$.

Nevertheless, if we use the phase difference of various antennas directly, then random noise and multiple-target reflections may also exist in the original signal, which would cause a large calculation error. Fortunately, we are able to extract the initial phase of each chirp in each frequency component by DFT. As introduced in Reference [1], we ignore the frequency deviation δ and white Gaussian noise $w[n]$ in Equation (5), and according to Equation (7), the phase of DFT samples could be transformed as:

$$\text{angle}(R[k]) = \begin{cases} \theta_0 & k = k_p \\ 0 & k \neq k_p \end{cases}, k = 0, 1, \ldots, N-1 , \tag{14}$$

where k_p is the DFT bin index with peak amplitude, and θ_0 is the initial phase of the corresponding frequency component. So, if frequency deviation $\delta = 0$ or we leave out the effect of δ, then we could read the initial phase by DFT results with peak point. Figure 9(a) illustrates a typical example with a sinusoidal signal: $x_1[n] = e^{j\left(2\pi f_1 n + \frac{\pi}{3}\right)}$, where frequency deviation $\delta = 0$. We illustrate the real part of x_1. As shown in Figure 9(b), we could extract the initial phase by the peak points of the DFT result X_1.

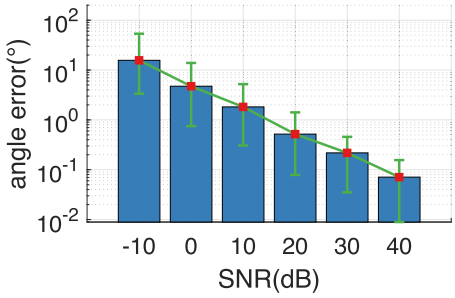

Fig. 10. Single-frequency signal estimation error of amplitude angle with respect to SNR.

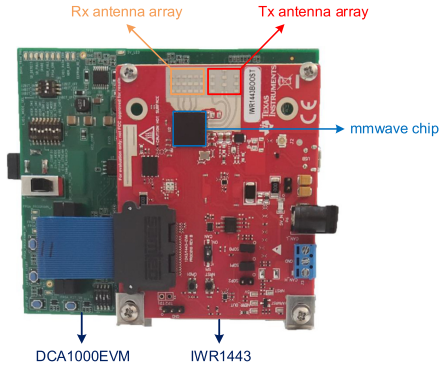

Fig. 11. Experiment device.

But in most cases, frequency deviation $\delta \neq 0$. Referring to Equation (7), the phase of peak point in the DFT spectrum could be written as follows:

$$\text{angle}(R[k_p]) = \theta_0 + \text{angle}(F(\delta)), \tag{15}$$

where $F(\delta) = \frac{1-e^{j2\pi\delta}}{1-e^{j\frac{2\pi}{N}\delta}}$ and $-\frac{1}{2} \leq \delta \leq \frac{1}{2}$.

Because $\text{angle}(F(\delta)) \neq 0$ when δ is not an integer, the initial phase that we extract from the peak point in the DFT spectrum would not accurate. Figure 9(c) is the real part of a sinusoidal signal: $x_2[n] = e^{j(2\pi f_2 n + \frac{\pi}{3})}$, where frequency deviation $\delta \neq 0$. In Figure 9(d), we find that the phase of peak point in DFT results X_2 is not equal to the initial phase of x_2.

Now, our goal is to estimate the initial phase θ_0 to calculate target AoA, which is derived from in Section 3.2. Hence, we get the initial phase from the estimated value θ_0 directly.

Figure 10 examines the error of initial phase θ_0 when we put up a single-frequency signal. We achieve the median angle error of less than 1° under SNR greater than 20 dB. Our algorithm estimates both the complex amplitude and normalized frequency deviation brilliantly.

Our AoA calculation algorithm is described as follows: For each receive antenna, we could obtain a set of target results. If there exists more than one target, then we match the range over antennas to obtain the parameter information of each target. Then, for each antenna, we could calculate phase θ_0 as the initial phase of each frequency component and figure out the AoA by Equation (13). Then, we obtain the location of targets in the 2-D plane by the range and AoA. To acquire height information, we need a 3-D antenna array. Antennas on the vertical direction give angular resolution in the vertical direction. Combining with target range, we are able to get 3-D localization. In our experiment, we use one Tx antenna and four Rx antennas on mmWave chip, which consist of a 2-D antenna array and only have the angular resolution in the horizontal direction. 3-D localization is left for our future work.

4 EVALUATION

4.1 Experimental Methodology

4.1.1 Implementation. We implement *milliLoc* on IWR1443BOOST [4] and DCA1000EVM [3] provided by TI company. As illustrated in Figure 11, IWR1443 integrates seven onboard antennas, including three Tx antennas (denoted as Tx1~Tx3) and four Rx antennas (denoted as Rx1~Rx4). The mmWave chip is around 1 cm × 1 cm. We utilize Tx1 to send FMCW signals sweeping from 77 GHz to 81 GHz and Rx1~Rx4 to receive the reflected signals. The chirp duration is set to 60 us

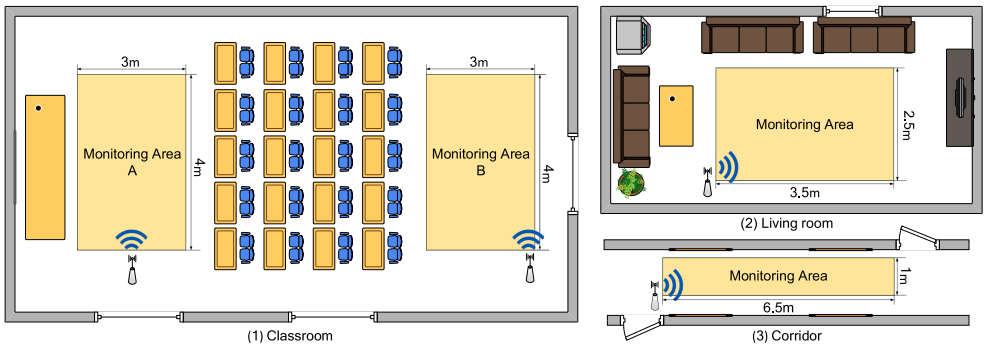

Fig. 12. Experiment setup in different scenarios.

and the number of samples per chirp is set to 256, corresponding to a maximum detection range of 10.2 m.

The samples are captured through DCA1000EVM via network cable in a high-speed and real-time manner. Moreover, we obtain ground truth by a lidar sensor [2]. We compare the 1-D range estimate results and AoA estimate results of *milliLoc* with ground truth to analyze the performance of our system. To facilitate the comparison of the estimate results with the ground truth and evaluate the system performance, we set the radio frame rate to 50 Hz, which means that the localization results are given every 0.02 second.

4.1.2 Evaluation Setup. We conduct experiments under three typical scenarios illustrated in Figure 12: a large empty classroom, a living room with various furniture, and a narrow corridor. In the classroom, we select two monitoring areas, and in the other two scenarios, we select one monitoring area, respectively, to comprehensively evaluate the performance of *milliLoc*.

Considering that if we take the human as the target, since the contour of the human body is a curved surface and all parts of the human body may reflect signals, it is not easy to accurately obtain the ground truth with millimeter-level accuracy. Consequently, we tie different boxes to a control car and monitor the localization and movements of the toy car under both static and dynamic conditions to evaluate the system performance.

4.2 System Performance

4.2.1 Single Target Localization Estimation Accuracy. We first compare the single target localization performance of *milliLoc* with the traditional and common method, "peak-pt" [1] and two state-of-the-art works, PDA [43] and GPR [23]. "peak-pt" uses the peak point directly to calculate the localization of the target. PDA calculates the cross-correlation function between the different sinusoidal kernel functions and the IF signal to estimate the localization. GPR computes the spatial heatmaps of the received signals based on the classical MUSIC algorithm and develops a Gaussian process regression model to compensate the systematic biases and detect the target location. We implement the algorithm of PDA and GPR and compare them with our system under the same environment and bandwidth.

Figure 13 shows the localization error of four approaches when a single target locates directly in front of mmWave device (AoA $< 5°$). *milliLoc* achieves a median localization accuracy of 5.5 mm, outperforming "peak-pt," PDA, and GPR. Compared to *milliLoc*, the median localization error of "peak-pt," PDA, and GPR are 11.1 mm, 10.2 mm, and 11.8 mm, respectively. As introduced in Section 2, the range resolution about "peak-pt" is around 4 cm. Assuming that the target has an equal probability of appearing in each location within the range bin, the localization error is a

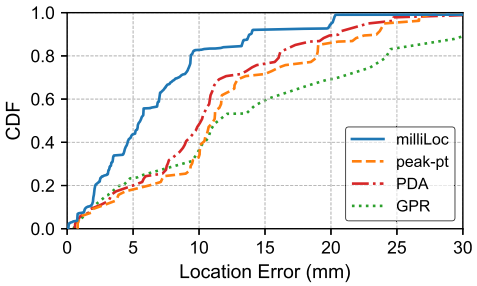

Fig. 13. Localization error when a single target locates directly in front of mmWave device.

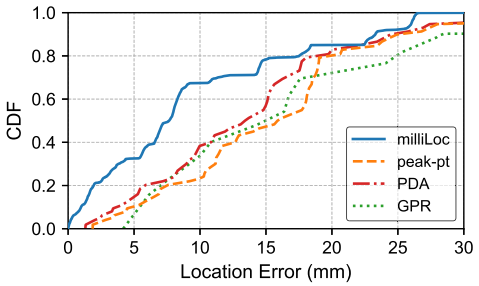

Fig. 14. Localization error when a single target locates diagonally in front of mmWave device.

uniform distribution from 0 to 2 cm. Consequently, the median localization error of "peak-pt" is theoretically about 1 cm. PDA and GPR capture the range of the target in terms of correlation function calculation and spatial resolution enhancement, respectively. However, PDA and GPR do not focus on the range resolution of a single target, thus falling short in improving the localization performance; while *milliLoc* makes full use of the IF frequency spectrum based on the spectral peak reconstruction algorithm and pushes the limit of the mmWave radar's ranging accuracy.

Figure 14 demonstrates the localization error when a single target locates diagonally in front of mmWave device (AoA > 5°). As shown, *milliLoc*, "peak-pt," PDA, and GPR achieve localization error of around 7.6 mm, 15.7 mm, 13.4 mm, and 14.9 mm, respectively. According to the law of reflection of electromagnetic waves, since the roughness of most targets is less than the wavelength of mmWave signal, the targets produce strong specular reflections to the incident mmWave signal. Consequently, most of the energy bounces off in the direction symmetric with the incidence angle. Because of the small antenna aperture of commercial mmWave radar, only if the signal arrives near the normal of the target surface, its reflection can be captured by the receive antennas [6, 8]. In total, when the AoA of the target increases, the signal reflected by targets may spread to other directions, and the signal received by mmWave device would be attenuated, which will lead to more noise interference and generate more inaccuracy during the solution of optimization. From the results, the localization performances of the above four methods all deteriorate as the AoA of the target increases. Nevertheless, *milliLoc* still achieves the best performance among the compared methods, which illustrates the effectiveness of our system.

4.2.2 Multiple Targets Localization Estimation Accuracy. We evaluate the localization performance with multiple targets. Figure 15 plots the localization error when two or three targets locate directly in front of mmWave device. As illustrated, *milliLoc* achieves higher performance with a median error of 11.3 mm and 17.7 mm for two-target and three-target scenarios, respectively. As the number of targets increases, the localization performance would decline due to the raising in interference between targets and the weakening of the reflected signals from certain targets. However, *milliLoc* could still achieve consistent localization performances for multiple targets.

4.2.3 AoA Estimation Accuracy. We compare AoA estimation accuracy of *milliLoc* against the common method, "peak-pt," and a state-of-the-art work, GPR. "peak-pt" uses the phase of peak point in range spectrum to calculate AoA directly, and GPR enhances the spatial resolution by applying Gaussian process regression on the MUSIC algorithm. Figure 16 shows the AoA estimation performance. *milliLoc* achieves a median error of 6.6°, which outperforms "peak-pt" with a median error of 9.6° and GPR with a median error of 8.5°, with a decrease of error by 31.2% and 22.3%. Due to the limited numbers of antennas of commercial devices, the thermal noise, and multi-path reflections during the practical environment [28, 44], the AoA measurement performances of the

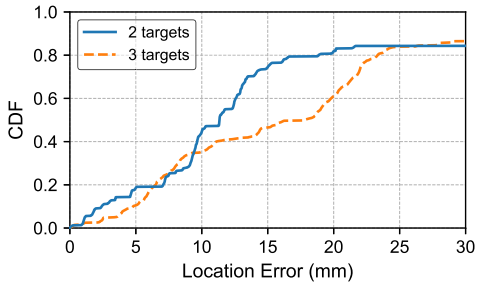

Fig. 15. Localization error when multiple targets locate directly in front of mmWave device.

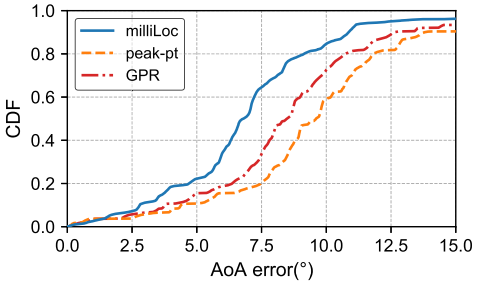

Fig. 16. AoA measure accuracy.

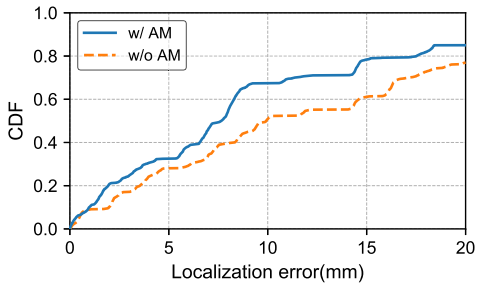

Fig. 17. Impact of amplitude modulation on location error.

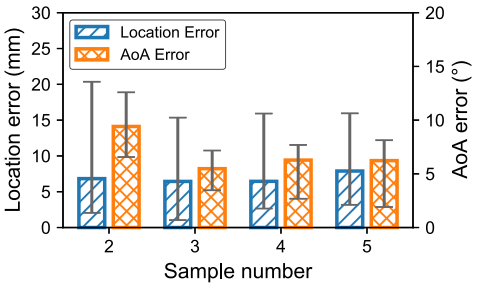

Fig. 18. Impact of sample number on location and AoA error.

above three methods both have a bit of deviations. With the application of the spatial resolution enhancement algorithm, the measurement error of AoA only has slight decline. However, *milliLoc* modifies the initial phase of each antenna by calculating the complex amplitude of the sinusoidal component, which improves the AoA measurement accuracy without extending the number of antenna arrays.

4.3 Parameter Study

4.3.1 Impact of Amplitude Modulation. In this experiment, we evaluate the performance of **amplitude modulation (AM)**, as introduced in Section 3.2. We compare the localization error with or without amplitude modulation. The results are shown in Figure 17. As can be seen, without amplitude modulation, the median localization error increases to 9.9 mm, and AM reduces the localization error by 23.2%. The results demonstrate that AM can diminish the disturbance of samples with lower amplitude and enhance the system performance.

4.3.2 Impact of Sample Number. In Section 3.2, we discuss that *milliLoc* needs at least two DFT samples to solve the optimization problem and acquire target range and AoA. We evaluate the performance when choosing different DFT sample numbers to calculate the location information. One single target is located directly in front of the mmWave device. Figure 18 shows the localization error and AoA error with various sample numbers, respectively. During the evaluation, we select DFT samples as close as possible to peak points to figure out the signal parameters with the purpose of bringing down the noise interference. As shown, the optimal sample number is three, which is an intermediate value in candidates. Even though we could solve the optimization problem by only two samples, it is less resistant to noise. If one sample suffers from stronger noise interference or calculation deviation, then the performance will deteriorate drastically. In our evaluation, the

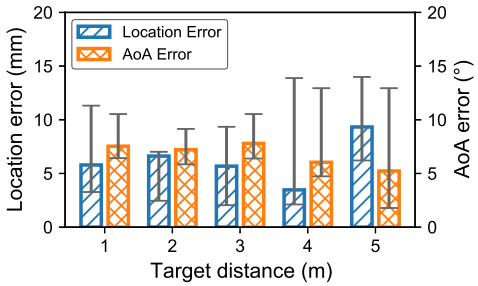

Fig. 19. Impact of target range on location and AoA error.

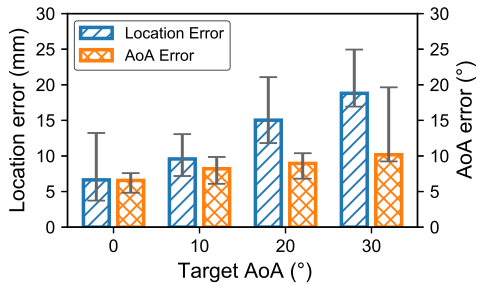

Fig. 20. Impact of target AoA on location and AoA error.

AoA error of two sample numbers grows significantly compared to other selections. Nevertheless, more than three sample numbers would bring up the error slightly. Considering that as the sample numbers increase, the amplitudes of the additional samples are commonly lower, and samples with lower amplitude are more susceptible to random noise and cause larger calculation errors during the process of solving. In addition, it will enhance the resource overhead. Consequently, the most appropriate choice is to use three samples to solve the optimization problem with only one frequency component.

4.3.3 Impact of Target Range. To evaluate the impact of the target range between the device and the target, we keep the target AoA to around 0° and change the distance between the target and mmWave device. Figure 19 shows the localization error and AoA error of *milliLoc*. As shown, when the distance changes from 1 m to 5 m, *milliLoc* achieves millimeter-level median localization error, and its median AoA error is less than 10°, which keeps consistent localization performances during various distances.

4.3.4 Impact of Target AoA. We further explore the impact of different target AoA. Figure 20 shows the localization error and AoA error. As shown, the range performance keeps stable at a low level with lower AoA. When target AoA is more than 20°, the localization error increases sharply. Similarly, the AoA performance deteriorates gradually with the target AoA augmenting. As introduced in Section 4.2.1, the reflection signal of targets would be attenuated and the environmental and hardware noise would compound the localization performance due to specular reflections to the mmWave signal as the target AoA increases.To achieve better localization performance of mmWave radar, we would better apply the system to the scenarios with lower AoA.

4.3.5 Impact of Different Targets. To determine whether *milliLoc* consistently works for different targets, we choose five boxes with different sizes to further evaluate the robustness of *milliLoc*. The sizes of different cuboid boxes are 29.7 cm × 6.8 cm × 18.4 cm, 16.8 cm × 5.8 cm × 13.0 cm, 20.0 cm × 5.3 cm × 17.5 cm, 21.0 cm × 4.2 cm × 14.0 cm, and 33.8 cm × 72 cm × 30.9 cm. Figure 21 demonstrates the localization error and AoA error of various targets. Results show that localization and AoA error may fluctuate slightly due to various box sizes. However, *milliLoc* achieves consistent performance across all targets.

4.3.6 Impact of Environments. The performance of *milliLoc* in different experiment environments is shown in Figure 22. Comparing the clusters, the performance of *milliLoc* is almost the same in different environments. Specifically, *milliLoc* achieves median localization and AoA error of around 6.0 mm and 7.0° in three various scenarios. It demonstrates that *milliLoc* is applicable in different environments, making our system more ubiquitous.

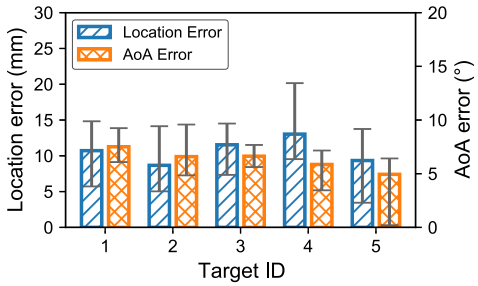

Fig. 21. Impact of different targets on location and AoA error.

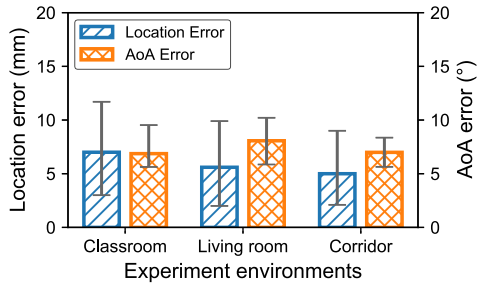

Fig. 22. Impact of experiment environments on location and AoA error.

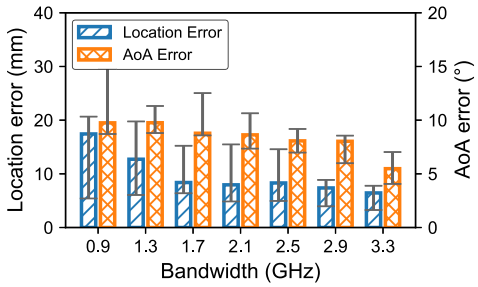

Fig. 23. Impact of bandwidth on location and AoA error.

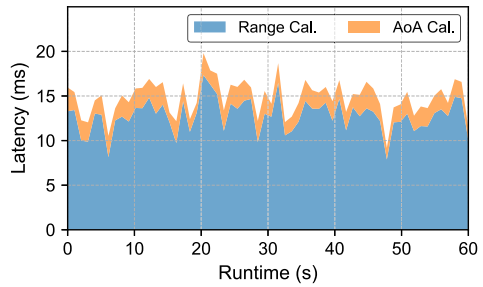

Fig. 24. System latency analysis.

4.3.7 Impact of Bandwidth. As demonstrated in Section 2, the available bandwidth is usually less than 4 GHz. We further evaluate the impact of bandwidth on system performance. The target is located directly in front of the mmWave device. From Equation (4), the range resolution will augment with the decreasing of bandwidth, so the localization error would increase when the bandwidth is reduced theoretically. From Figure 23, localization error will rise significantly with bandwidth decreasing. Similar to the localization performance, the AoA performance would decline with the decreasing bandwidth. When the bandwidth decreases to 0.9 GHz, the median localization error and AoA error drop to 17.4 mm and 9.4°, respectively. When the bandwidth decreases, the range resolution will deteriorate and the random noises in the IF frequency spectrum will be amplified, which enlarges the calculation error of complex amplitude of sinusoidal component and brings down the AoA performance. To achieve better results, we are supposed to apply the maximum bandwidth to the experiment.

4.3.8 System Latency Analysis. To validate the efficiency of *milliLoc*, we further evaluate the system latency. The system is running on a laptop with 8 cores of Intel i7-6700HQ CPU @ 2.60 GHz. Figure 24 illustrates the end-to-end latency of *milliLoc*, including range calculation delay and AoA calculation delay. As shown, the average end-to-end latency is 14.6 ms, with an average of 13.1 ms for range calculation and 1.5 ms for AoA calculation. The results show that most of the system latency is induced by the *spectral peak reconstruction algorithm*, especially the optimization process. To conclude, the latency evaluation results indicate *milliLoc* can achieve real-time calculation for the radio frame rate of 50 Hz.

5 DISCUSSION

In this work, we propose a millimeter-level multi-target localization system based on COTS mmWave radar, and there are some notes and future directions to extend our work, which we discuss below.

Localization of multiple targets. In Section 4.2, we evaluate the system performance when two or three targets locate in the monitoring area. In theory, the multi-target localization algorithm we proposed in Section 3.3 is able to localize more targets simultaneously. However, when the number of targets increases, the reflection signal of certain targets may be diminished, and different targets may even occlude each other, which causes the degradation of localization performance. We believe that the temporal continuity of target motion can contribute to reducing the impact of the above interference. By integrating the continuity of distance changes between adjacent moments and the measurement of the mmWave device, we are capable of mitigating the influence of signal interference. We leave it for future work.

Localization of different kinds of targets. In Section 4.1, we tie boxes with various sizes to a control car and change the location of boxes by monitoring the control car to capture the ground truth with millimeter-level localization accuracy and evaluate the system performance precisely. Among existing works, mTrack [37] utilizes a PC host to control the remote movement of the target (e.g., a pen) and obtain the millimeter-level ground truth, while mmTrack [40] uses pre-marked trajectories as the ground truth, which can achieve centimeter-level accuracy for person localization. However, PC-controlled movements usually have a small monitoring area, and pre-marked trajectories are difficult to acquire more precise localization results. The above two schemes are tough applied to the evaluation of our system. In fact, our system can locate various types of targets. Combined with the 3-D antenna array, we can obtain the distance distribution profile in both the vertical and horizontal directions and further get the target meshes, which remains an important topic for further research.

6 RELATED WORK

In this section, we briefly summarize the most related works in the following categories.

RF-based active localization. Active localization requires targets to carry dedicated devices to transmit or receive RF signals for localization, including RFID tags [34, 45], mobile phones [16, 17, 21, 31, 39, 49], and wearable devices [11, 12]. RIM [39] and SpotFi [16] both build a complex antenna array and use Wi-Fi signals for target locating. For sound-based active localization, CAT [21] combines Doppler shifts estimated by the acoustic signal and measurements provided by the Inertial Measurement Unit to enhance the localization accuracy. Vernier [49] reduces the tracking delay and overhead by removing the complex frequency analysis process and derives moving distance directly by the phase change of sound signal. RF-IDraw [34] and Tagoram [45] adopt RFID tags for target tracking. However, systems based on active localization are not applicable to some scenarios, such as intruder detection. In addition, multiple-target localization requires a large number of dedicated devices, which calls for a large financial expense. In contrast, *milliLoc* could achieve target localization without any specific device carried by targets, which is convenient for applying to more scenarios and reduces the utilization of dedicated devices.

RF-based passive localization. Passive localization employs reflection signals to detect and track targets, including acoustic signals, Wi-Fi signals, and mmWave signals. VoLoc [32] designs an iterative cancellation algorithm for AoA estimation through the multipath of acoustic signal, followed by joint optimization of user distance and orientation. LLAP [36] exploits the phase changes of sound signals caused by target movements and transfers the phase changes into the displacement, which achieves millimeter-level accuracy within a 30 cm range. Strata [46]

estimates the **channel impulse response (CIR)** to tackle multi-path propagation and extracts the phase change of the corresponding tap to estimate the distance change. Wi-Fi-based localization work usually utilizes sundry channel parameters from finer-grained CSI other than RSSI to locate the target, including **Angle of Arrival (AoA), Time of Flight (ToF)**, and **Doppler Frequency Shifts (DFS)** [14, 25]. Some works jointly estimate multiple parameters to achieve better accuracy [15, 20, 27, 41]. Reference [47] proposes a metric called SSNR to quantify the signal sensing capability and strengthens the reflection signal by multiple antennas to increase the Wi-Fi sensing range. Despite that existing localization systems are able to locate and track targets, most do not achieve higher localization accuracy. Wi-Fi-based solutions could achieve decimeter-level accuracy generally due to the limitation of bandwidth and antenna number. Sound-based systems usually have a small coverage area and deteriorate under noise surroundings due to lower input SNR. Lidar-based localization methods [35] usually need expensive equipment and they could not work normally under adverse weather conditions, such as fog and sandstorm.

Recently, mmWave devices have attracted increasing interest, which are exploited to target localization. mmTrack [40] and Reference [38] utilize 60 GHz Wi-Fi technology and 24 GHz FMCW radar to accomplish multiple persons tracking, respectively, which could achieve decimeter-level accuracy. mTrack [37] designs a 60 GHz Wi-Fi system to track writing objects with signal phase shifting but it only works well within a limited range. Osprey [24] devises an inverse synthetic aperture radar algorithm that exploits the natural rotation of the tire and measures accurate tire wear. Nevertheless, those works do not concentrate on the limited range resolution of mmWave radar. mmVib [13] proposes a multi-signal consolidation model, which describes the properties of reflected mmWave signals to capture the sub-millimeter-level vibrations. However, It can only sense displacements smaller than the signal wavelength and can not obtain precise absolute range. Compared with these works, *milliLoc* could achieve millimeter-level localization accuracy by pushing the limit of range resolution of mmWave radar without the movement of the target.

Super-resolution algorithms. Researchers put forward many super-resolution techniques, including MUSIC [30], ESPRIT [29]. The MUSIC [30] algorithm utilizes a linear antenna array and calculates the power spectral density function in different directions to get the directions of arrival. The ESPRIT [29] algorithm designs a signal parameter estimation method based on total least-squares, which could be used to direction-of-arrival estimation and system identification. Based on these classical super-resolution algorithms, new localization methods are proposed. Ubicarse [18] is able to perform synthetic aperture radar on handheld devices twisted by the users along unknown paths. It allows mobile devices to emulate an antenna array. D-MUSIC [26] eliminates the unknown phase offsets on COTS Wi-Fi devices with only one rotation and achieves accurate AoA estimation. GPR [23] calculates the range-velocity and range-azimuth heatmaps based on the MUSIC algorithm and implements Gaussian process regression to refine the range and the angular localization of the target. It demands pre-collected data to train the Gaussian process regression model before usage. Different from existing works that only concentrate on increasing spatial resolution, our algorithm attempts to push the limit of frequency resolution to make the localization results more accurate.

Zero-padded DFT [10] only improves the sampling density of the spectrum. It does not change the frequency resolution and could not distinguish adjacent multiple frequencies. In addition, it does not calculate the amplitude of each frequency component, which could not figure out the AoA of targets. PDA [43] sets different sinusoidal functions as kernel functions and conducts the correlation calculation with the received signal to achieve the de-alternating performance and estimate the signal frequency. Essentially, the measurement accuracy of the scheme is still limited by the signal bandwidth. Compared with these methods, our system pushes the limit of mmWave

radar-based localization by more accurate frequency estimation during single-target and multiple-target situations and improves the AoA estimated accuracy by complex amplitude.

7 CONCLUSION

In this article, we propose *milliLoc*, a millimeter-level multi-target localization system based on COTS mmWave radar. *milliLoc* pushes the limit of the mmWave ranging accuracy by leveraging a novel-designed *spectral peak reconstruction algorithm*, then innovatively utilizes the complex amplitude information to improve the accuracy of AoA measurement. Based on our further extension, *milliLoc* could handle both the single-target and the multi-target situations. Extensive evaluation results show that *milliLoc* achieves millimeter-level localization accuracy and decreases the AoA measure error by 31.2%. Our system can be easily integrated with other existing solutions, thus taking a promising step towards high-accuracy location-based applications.

REFERENCES

[1] Sandeep Rao. 2020. Introduction to mmWave Sensing: FMCW Radars. Retrieved from https://training.ti.com/sites/default/files/docs/mmwaveSensing-FMCW-offlineviewing.pdf.

[2] Livox Technology. 2020. Livox Mid-40 LiDAR. Retrieved from https://www.livoxtech.com/mid-40-and-mid-100.

[3] Texas Instruments. 2020. Texas Instruments DCA1000EVM. Retrieved from https://www.ti.com/tool/DCA1000EVM.

[4] Texas Instruments. 2020. Texas Instruments IWR1443BOOST. Retrieved from https://www.ti.com/tool/IWR1443BOOST.

[5] Fadel Adib, Zachary Kabelac, and Dina Katabi. Multi-person localization via RF body reflections. In *Proceedings of USENIX NSDI*.

[6] Sherif Sayed Ahmed and Lorenz-Peter Schmidt. 2012. Illumination of humans in active millimeter-wave multistatic imaging. In *Proceedings of IEEE EUCAP*.

[7] Donald E. Barrick. 1973. *FM/CW Radar Signals and Digital Processing*. US Department of Commerce, National Oceanic and Atmospheric Administration.

[8] Ciro Cafforio, Claudio Prati, and Fabio Rocca. 1991. SAR data focusing using seismic migration techniques. *IEEE Trans. Aerosp. Electron. Syst.* 27, 2 (1991).

[9] Quin Cai and Jake K. Aggarwal. 1998. Automatic tracking of human motion in indoor scenes across multiple synchronized video streams. In *Proceedings of IEEE ICCV*.

[10] Codrin Donciu and Marinel Temneanu. 2015. An alternative method to zero-padded DFT. *Elsev. Meas.* 70 (2015).

[11] Michael Hardegger, Daniel Roggen, and Gerhard Tröster. 2015. 3D ActionSLAM: Wearable person tracking in multi-floor environments. *Proc. Springer Person. Ubiq. Comput.* 19 (2015).

[12] Michael Hardegger, Gerhard Tröster, and Daniel Roggen. 2013. Improved actionSLAM for long-term indoor tracking with wearable motion sensors. In *Proceedings of ACM ISWC*.

[13] Chengkun Jiang, Junchen Guo, Yuan He, Meng Jin, Shuai Li, and Yunhao Liu. 2020. mmVib: Micrometer-level vibration measurement with mmWave radar. In *Proceedings of ACM MobiCom*.

[14] Kiran Joshi, Dinesh Bharadia, Manikanta Kotaru, and Sachin Katti. 2015. WiDeo: Fine-grained device-free motion tracing using RF backscatter. In *Proceedings of USENIX NSDI*.

[15] Chitra R. Karanam, Belal Korany, and Yasamin Mostofi. 2019. Tracking from one side: Multi-person passive tracking with WiFi magnitude measurements. In *Proceedings of IEEE/ACM IPSN*.

[16] Manikanta Kotaru, Kiran Joshi, Dinesh Bharadia, and Sachin Katti. 2015. SpotFi: Decimeter level localization using WiFi. In *Proceedings of ACM SIGCOMM*.

[17] Manikanta Kotaru and Sachin Katti. 2017. Position tracking for virtual reality using commodity WiFi. In *Proceedings of IEEE CVPR*.

[18] Swarun Kumar, Stephanie Gil, Dina Katabi, and Daniela Rus. 2014. Accurate indoor localization with zero start-up cost. In *Proceedings of ACM MobiCom*.

[19] Kenneth Levenberg. 1944. A method for the solution of certain non-linear problems in least squares. *Quart. Appl. Math.* 2, 2 (1944).

[20] Xiang Li, Daqing Zhang, Qin Lv, Jie Xiong, Shengjie Li, Yue Zhang, and Hong Mei. 2017. IndoTrack: Device-free indoor human tracking with commodity Wi-Fi. *Proc. ACM IMWUT* 1, 3 (2017).

[21] Wenguang Mao, Jian He, and Lili Qiu. 2016. CAT: High-precision acoustic motion tracking. In *Proceedings of ACM MobiCom*.

[22] Donald W. Marquardt. 1963. An algorithm for least-squares estimation of nonlinear parameters. *J. Societ. Industr. Appl. Math.* 11, 2 (1963).

[23] José A. Paredes, Fernando J. Álvarez, Miles Hansard, and Khalid Z. Rajab. 2021. A Gaussian process model for UAV localization using millimetre wave radar. *Expert Syst. Applic.* 185 (2021).
[24] Akarsh Prabhakara, Vaibhav Singh, Swarun Kumar, and Anthony Rowe. 2020. Osprey: A mmWave approach to tire wear sensing. In *Proceedings of ACM MobiSys*.
[25] Kun Qian, Chenshu Wu, Zheng Yang, Yunhao Liu, and Kyle Jamieson. 2017. Widar: Decimeter-level passive tracking via velocity monitoring with commodity Wi-Fi. In *Proceedings of ACM MobiHoc*.
[26] Kun Qian, Chenshu Wu, Zheng Yang, Zimu Zhou, Xu Wang, and Yunhao Liu. 2016. Tuning by turning: Enabling phased array signal processing for WiFi with inertial sensors. In *Proceedings of IEEE INFOCOM*.
[27] Kun Qian, Chenshu Wu, Yi Zhang, Guidong Zhang, Zheng Yang, and Yunhao Liu. 2018. Widar2. 0: Passive human tracking with a single Wi-Fi link. In *Proceedings of ACM MobiSys*.
[28] Sai Deepika Regani, Chenshu Wu, Beibei Wang, Min Wu, and K. J. Ray Liu. 2021. mmWrite: Passive handwriting tracking using a single millimeter-wave radio. *IEEE InternetThings J.* 8, 17 (2021).
[29] Richard Roy and Thomas Kailath. 1989. ESPRIT-estimation of signal parameters via rotational invariance techniques. *IEEE Trans. Acoust. Speech.d Sig. Process.* 37, 7 (1989).
[30] Ralph Schmidt. 1986. Multiple emitter location and signal parameter estimation. *IEEE Trans. Ant. Propag.* 34, 3 (1986).
[31] Souvik Sen, Jeongkeun Lee, Kyu-Han Kim, and Paul Congdon. 2013. Avoiding multipath to revive inbuilding WiFi localization. In *Proceedings of ACM MobiSys*.
[32] Sheng Shen, Daguan Chen, Yu-Lin Wei, Zhijian Yang, and Romit Roy Choudhury. 2020. Voice localization using nearby wall reflections. In *Proceedings of ACM MobiCom*.
[33] Duraisamy Sundararajan. 2001. *The Discrete Fourier Transform: Theory, Algorithms and Applications*, World Scientific.
[34] Jue Wang, Deepak Vasisht, and Dina Katabi. 2014. RF-IDraw: Virtual touch screen in the air using RF signals. In *Proceedings of ACM SIGCOMM*.
[35] Liang Wang, Yihuan Zhang, and Jun Wang. 2017. Map-based localization method for autonomous vehicles using 3D-LIDAR. *ElsevierIFAC* 50, 1 (2017).
[36] Wei Wang, Alex X. Liu, and Ke Sun. 2016. Device-free gesture tracking using acoustic signals. In *Proceedings of ACM MobiCom*.
[37] Teng Wei and Xinyu Zhang. 2015. mTrack: High-precision passive tracking using millimeter wave radios. In *Proceedings of ACM MobiCom*.
[38] Christoph Will, Prachi Vaishnav, Abhiram Chakraborty, and Avik Santra. 2019. Human target detection, tracking, and classification using 24-GHz FMCW radar. *IEEE Sensors J.* 19, 17 (2019).
[39] Chenshu Wu, Feng Zhang, Yusen Fan, and K. J. Ray Liu. 2019. RF-based inertial measurement. In *Proceedings of ACM SIGCOMM*.
[40] Chenshu Wu, Feng Zhang, Beibei Wang, and K. J. Ray Liu. 2020. mmTrack: Passive multi-person localization using commodity millimeter wave radio. In *Proceedings of IEEE INFOCOM*.
[41] Yaxiong Xie, Jie Xiong, Mo Li, and Kyle Jamieson. 2019. mD-Track: Leveraging multi-dimensionality for passive indoor Wi-Fi tracking. In *Proceedings of ACM MobiCom*.
[42] Jie Xiong and Kyle Jamieson. 2013. ArrayTrack: A fine-grained indoor location system. In *Proceedings of USENIX NSDI*.
[43] Yuyong Xiong, Shiqian Chen, Guanpei Xing, Zhike Peng, and Wenming Zhang. 2018. High-precision frequency estimation for FMCW radar applications based on parameterized de-alternating and modified ICCD. *Measur. Sci. Technol.* 29, 7 (2018).
[44] Jingao Xu, Guoxuan Chi, Zheng Yang, Danyang Li, Qian Zhang, Qiang Ma, and Xin Miao. 2021. FollowUpAR: Enabling follow-up effects in mobile AR applications. In *Proceedings of ACM MobiSys*.
[45] Lei Yang, Yekui Chen, Xiang-Yang Li, Chaowei Xiao, Mo Li, and Yunhao Liu. 2014. Tagoram: Real-time tracking of mobile RFID tags to high precision using COTS devices. In *Proceedings of ACM MobiCom*.
[46] Sangki Yun, Yi-Chao Chen, Huihuang Zheng, Lili Qiu, and Wenguang Mao. 2017. Strata: Fine-grained acoustic-based device-free tracking. In *Proceedings of ACM MobiSys*.
[47] Youwei Zeng, Jinyi Liu, Jie Xiong, Zhaopeng Liu, Dan Wu, and Daqing Zhang. 2021. Exploring multiple antennas for long-range WiFi sensing. *Proc. ACM IMWUT* 5, 4 (2021).
[48] Chi Zhang and Xinyu Zhang. 2017. Pulsar: Towards ubiquitous visible light localization. In *Proceedings of ACM MobiCom*.
[49] Yunting Zhang, Jiliang Wang, Weiyi Wang, Zhao Wang, and Yunhao Liu. 2018. Vernier: Accurate and fast acoustic motion tracking using mobile devices. In *Proceedings of IEEE INFOCOM*.

Received 2 April 2022; revised 15 August 2022; accepted 13 October 2022